 doi:10.20944/preprints202201.0041.v1

Article

Strengthening of Reinforced Concrete Beams Subjected to Concentrated Loads

Paolo Foraboschi*

Dipartimento di Culture del Progetto – Università IUAV di Venezia (Venice; Italy) E-Mail: paofor@iuav.it

Abstract: Renovation, restoration, remodeling, refurbishment, and retrofitting of buildings often imply modifying the behavior of the structural system. Modification sometimes includes applying forces (i.e., concentrated loads) to beams that before were subjected to distributed loads only. For a reinforced concrete structure, the new condition causes a beam to bear a concentrated load with the crack pattern that was produced by the distributed loads that acted in the past. If the concentrated load is applied at or near the beam's midspan, the new shear demand reaches the maximum around the midspan. But around the midspan, the cracks are vertical or quasi-vertical, and no inclined bar is present. So, the actual shear capacity around the midspan not only is low, but also can be substantially lower than the new demand. In order to bring the beam capacity up to the demand, fiber-reinforced-polymer composites can be used. This paper presents a design method to increase the concentrated load-carrying capacity of reinforced concrete beams whose load distribution has to be changed from distributed to concentrated, and an analytical model to predict the concentrated load-carrying capacity of a beam in the strengthened state.

Keywords: : building remodeling; concentrated loads; FRP reinforcement; FRP strips; shear capacity; vertical concrete cantilever

1. Introduction

There is a time of their service life at which any construction does not meet any longer the modern architectural demand. At that time, the construction may be subjected to renovation, restoration, remodeling, refurbishment or retrofitting, in order to meet the modern demand (apart from monumental buildings).

Those activities may include placing new columns, walls, beams or trusses into the building. The new structural elements may be made supported by existing beams that before carried a structural floor or slab. Moreover, the new elements may be placed at, or near, the midspan of the existing beam. In doing so, a beam that was subjected to distributed loads will be subjected to a concentrated load applied around the midspan.

If the beam is made of Reinforced Concrete (RC), the new loading condition is demanding even if the concentrated load does not exceed the resultant force of the previous distributed load. In fact, the loads that have acted on the beam since its construction caused concrete to crack and cracking is stabilized when the load distribution is changed. Ergo, the RC beam has to carry a concentrated load around the midspan with the crack pattern due to the distributed loads. That condition implies a weakness that often requires strengthening the beam.

This paper is devoted to existing Reinforced Concrete (RC) beams whose applied load distribution is changed from distributed to concentrated and presents a design method to increase the concentrated load-carrying capacity, including the analytical model that predicts the increase.

 doi:10.20944/preprints202201.0041.v1

2. Statement of the issue being addressed

This paragraph is devoted to framing the topic this paper deals with and to presenting the study's statement of purpose which all elements of the paper relate logically to.

2.1. Starting knowledge

A lot of research work has been accomplished since the end of the nineteenth century on the shear behavior of RC structures and outstanding papers are available in the literature.

An essential advance in knowledge is the well-known analogy between the shear strength of a web-reinforced concrete beam and a flat truss, postulated by Ritter (1899) [1], disseminated by Mörsch in Europe (1902) [2-4], and introduced into the American literature by Withey (1907) [5].

Another significant advance in knowledge is the strut-and-tie modeling, which divides a structure in B-regions ("B" standing for beam or Bernoulli) and D-regions ("D" standing for discontinuity or disturbed). The latter are in the vicinity of loads or geometric discontinuities, while the former are between the latter. Only the analysis and design of B-regions can proceed on a sectional basis for which plane sections remain plane while the analysis and design of D-regions must proceed on a regional basis. Some of the many references are [6-27].

Then, a lot of research activity has been devoted to studying the beam action and the arch action in the shear span. Some of the many references are [28-44].

2.2. Flat truss analogy: review

The principal theoretical shear resisting system of a RC structure is an ideal parallel chord truss made of concrete and steel. The truss is composed of a top compression chord (the concrete from the neutral axis to the compression edge, together with the steel longitudinal reinforcement included into that region), a bottom tension chord (the steel longitudinal flexural reinforcement), vertical tension ties (closed steel stirrups that span from the top chord to the bottom chord, sometimes with the addition of bent-up longitudinal steel bars, and/or inclined steel bars), and 45° inclined compression struts (the concrete between the shear cracks).

The joints of the members that compose the truss are assumed to be hinges. Accordingly, that system is called 'pin-joined truss'. The pin-joined truss is statically determinate and stable. Consequently, the axial force in the truss's components can be calculated using the equilibrium only.

The truss mechanism exists only after the formation of the shear cracks, which cause the diagonal tension stresses to disappear.

2.3. Typical cracking pattern of existing RC beams

This point reviews the cracking behavior of a simply-supported RC beam with web-reinforcement, under uniform loading. The review includes some extensions to the doubly-fixed RC beam [32, 37, 45-49].

A uniform load induces a two-dimensional state of stress in the beam. If the maximum principal stress exceeds the concrete tensile strength, it causes concrete to crack.

At the midspan, the principal stresses are dictated by the bending moment only (this is also true for the doubly-fixed RC beam). Therefore, the principal stresses act on vertical planes and reach their maximum at the bottom of the cross-section. Thus, a crack at the midspan initiates at the bottom face of the beam and propagates upwards vertically, reaching the compression zone in the upper part of the cross-section (flexural crack).

From the midspan to the supports the interaction between bending moment and shear force increases. However, cracks are still initiated by bending moment, unless the beam is particularly deep. Each of those cracks starts hence from the bottom face of the beam and propagates upwards. Nonetheless, the shear force is not nil. So, propagation is

driven by both bending and shear. Those cracks exhibit a deviation from verticality (flexural-shear cracks). Deviation increases from around the midspan, where cracks are quasi-vertical, to the supports, where crack inclination is approximately 45°.

Around a support of a simply-supported RC beam, the principal stresses are dictated by the shear force. Thus, the principal stresses act on planes at 45° and reach their maximum at the centroid. A crack due to shear force initiates at the centroid and propagates at 45°, reaching the bottom edge of the beam (shear crack).

Ultimately, the crack pattern of a simply-supported RC beam exhibits vertical cracks at the midspan, quasi-vertical cracks around the midspan, and progressively more splayed cracks toward the supports.

At and near the supports of a doubly-fixed RC beam there is some interaction between shear and bending. As a result, cracks can be either vertical (flexural cracks that initiate at the top edge) or at 45° (shear cracks).

There is however much less chance of cracks that initiate at the centroid of the cross-section (shear cracks) appearing around the supports, whatever the restraints.

2.4. Typical steel reinforcement around the midspan

The intended structural use of the vast majority of the beams is to bear uniformly distributed loads. Accordingly, the steel reinforcement around the midspan of the vast majority of the RC beams consists of longitudinal bars (at the top and bottom of the cross-section) and relatively widely spaced stirrups. Neither bent-up longitudinal bars nor inclined tension ties are present around midspan, since the distributed loads imply that the shear force is low around midspan.

This paper deals with existing RC beams that were designed to bear uniform loads. Around the midspan of the beams that are dealt with herein, hence, the steel reinforcement has the above-described pattern.

2.5. Shear capacity of the beam around the midspan

The pin-joined truss analogy does not allow the inclination of the concrete struts to be chosen but requires that each strut consists in the concrete between two consecutive cracks, while it cannot intersect a crack. Namely, the inclination of the concrete struts has to be that of the cracks. If a concrete crack intersected a crack, in fact, it could not close the crack it intersects, which would imply that the concrete strut does not transmit any compression force, which in turn would imply that the truss is unstable.

Ergo, the pin-joined truss analogy is valid only around the supports, not at midspan. Nevertheless, around the supports the shear force is maximum while around midspan is minimum. So, the pin-joined truss analogy allows the shear capacity of RC structure to be calculated and guaranteed where it can dictate the load-carrying capacity of the beam.

Given that a strut has to coincide with the concrete between two consecutive cracks, away from the beam's support the classical pin-joined truss analogy (whose concrete struts are at 45°) has to be replaced by a pin-joined truss whose concrete struts have inclination that progressively decreases from a support towards the midspan.

Around the midspan of such a pin-joined truss, however, a concrete strut and the steel stirrup following one after the other have not only the same inclination (vertical) but also the same position. Thus, the segment of pin-joined truss with vertical concrete struts and web reinforcement is unstable.

Ultimately, neither the classical pin-joined truss analogy nor the modified pin-joined truss justifies any shear capacity of the beam's segment where cracks are vertical. However, the pin-joined truss analogy loses its validity only where the shear demand of a distributed load is low, so this deficiency can be ignored for the vast majority of the RC beams.

Neither the fact that the pin-joined truss analogy does not hold true, nor the absence of web reinforcement automatically entails that a RC beam fails [14-16, 21, 24,25, 32, 35, 37, 41, 54]. It depends on which internal action will initiate cracking.

Around the midspan and in the case of RC beams without web reinforcement, if cracking is initiated by the shear force, the crack propagates inclined along the entire height, up to severing the beam. Ergo, a shear crack causes failure. So, the beam cannot bear the load that has cracked the concrete. If cracking is initiated by the bending moment, the crack propagates either vertically or inclined along the section, up to stabilization (as long as the amount of tension reinforcement is adequate). Ergo, flexural cracks and flexural-shear cracks allow a stabilized crack pattern to be reached. So, the beam can bear the load that has cracked the concrete.

The shear resistant mechanisms of a RC beam with flexural cracks and without web reinforcement are the beam action and the arch action [6-27].

The arch action consists in an ideal concrete arch, given by the internal compression. The shear capacity derives from the inclination of the internal compression, which is substantial at the support but negligible around the midspan. So, the arch action provides the segment around the midspan with marginal shear capacity.

The beam action triggers when the cracks divide the tension zone into blocks, each of which consists in the concrete between two consecutive cracks. A block is referred to as 'concrete cantilever', since it acts as a cantilever with the base at the compression zone of the concrete and the free end in the concrete cover, and with the bond force variation applied at the free end.

The beam action mechanism can transfer the transverse shear force in the uncracked cross-sections and the bond force variation between two consecutive cracks.

In every RC beam, the transverse shear force of a shear cracked or flexural-shear cracked section is resisted by means of tangential stresses acting on the uncracked concrete of the cracked cross-section, boosted by dowel action and aggregate interlock. Thus, the shear force is equilibrated by shear stresses in the concrete, on the crack mouths, and in the longitudinal tension reinforcement, plus the vertical force in the stirrup if the beam has the web reinforcement.

In a beam without web reinforcement failure occurs in a brittle mode, since it is dictated by concrete tensile strength. At failure, thus, the transverse relative displacements between the crack faces are small. Therefore, dowel action and aggregate interlock boost no more than moderately the shear transfer across the uncracked concrete zone of a cracked cross-section.

In every RC beam, the bond force variation between two consecutive shear cracks or flexural-shear cracks is resisted by means of the strength of the concrete cantilever, boosted by dowel action and aggregate interlock.

Even in a beam without web reinforcement, failure of the concrete cantilever occurs in a relatively ductile mode, because it is governed by bending. If the tensile strength of the concrete cover and the flexural stiffness of the longitudinal reinforcement are substantial, the dowel force transferred across the cracks by the flexural reinforcement can be significant. Moreover, if the width of the two faces of a crack is no more than moderate, the shear stresses transferred across the crack by means of interlocking is large.

Of course, the contributions of dowel action and aggregate interlock are much greater for beams with web reinforcement, which provides the cover with extra tensile strength and keeps the cracks sufficiently closed. Nevertheless, for beams without web reinforcement those contributions can be significant too.

Unfortunately, the contributions of dowel action and aggregate interlock are minor in the case of flexural cracks, i.e., around the midspan. The reason is that the more vertical a crack and a concrete cantilever, the less the transverse relative displacements between the crack faces, for a given bending displacement of the cantilever.

Where the cracks are vertical, thus, the transverse relative displacements of the faces of a crack are slight and consequently the contributions of dowel action and aggregate interlock is negligible.

Ultimately, the shear force due to a concentrated load applied in a zone of the beam with vertical cracks (around the midspan) is maximum, while the shear strength is provided only by the uncracked concrete and consequently is small.

2.6. Gap statement and research problem

According to the conclusion of paragraph 2.5, changing the load distribution of a RC beam often require strengthening the beam in order to increase the shear strength.

Increasing the shear strength of a segment of a RC beam with vertical cracks requires referring to a model different than the pin-joined truss (neither the classical analogy nor the truss with struts whose inclination varies can simulate that shear behavior). Moreover, neither the dowel action nor the aggregate interlock provides a significant contribution.

Ultimately, the model that can be borrowed from literature and codes do not allow the concentrated load-carrying capacity to be modeled and predicted. That is the gap in knowledge that this paper aims to fill.

2.7. Study's statement of purpose and basic reference beam

The focus of the present research activity was to define a method for increasing the concentrated load-carrying capacity of RC beams, including an analytical model that predicts the capacity in the strengthened state.

The RC beams considered here are existing. That is, the beams are cracked and cracking is stabilized, and they do not have any reinforcement purposely designed for resisting concentrated loads around the midspan, which are the typical conditions.

The content and the results of this paper, including the analytical model, apply to any RC beam. However, a reference structure saves the potential readers to invest too much effort in understanding the paper and, on the other hand, does not imply losing generality.

The basic reference structure is the beam diagrammed in Fig. 1. The adopted reference structure schematizes the beams of buildings and bridges.

The cross-section of the reference beam is constant, and the restraints are symmetric. The reference beam has tee cross-section (T-beam). Hence, the model includes directly the prismatic simply-supported (Fig. 1) and doubly-fixed beams. Nevertheless, the model can be easily extended to non-prismatic beams and non-symmetric restraints (fixed-roller beam).

Preprints (www.preprints.org) | NOT PEER-REVIEWED | Posted: 5 January 2022 doi:10.20944/preprints202201.0041.v1

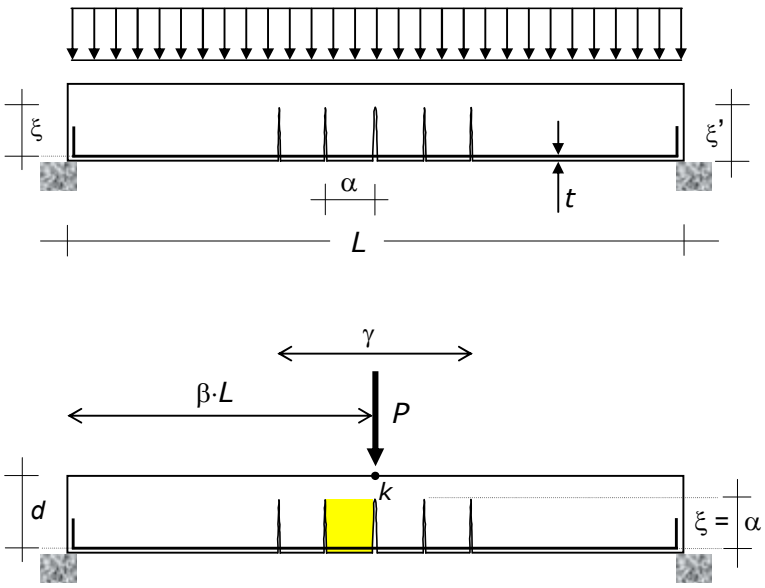

Figure 1. RC beam with vertical cracks around the midspan, which are spread along the length γ at spacing α. The upper diagram shows the loading condition that acted in the past and that cracked the beam, i.e., a distributed load. The lower diagram shows the new loading condition, i.e., a concentrated load *P* applied at a point *K* (which the figure places at the midspan, but that can be anywhere along *L*. Its position is defined by β). The shadowed concrete cantilever (or the symmetric one) dictates the failure of the RC beam under the concentrated load *P*. The figure also shows the span *L*, the depth *t* of the concrete cover, the crack depth ξ, and the effective crack depth ξ'.

3. Shear strengthening of RC beams

Shear strengthening of RC beams poses serious concerns with traditional techniques [59-63]. An innovation of the nineties of the past century was externally bonded Fiber-Reinforced Polymer (FRP) systems [64-66].

FRP systems for strengthening RC structures are an alternative to traditional strengthening techniques such as steel plate bonding, section enlargement, and external post-tensioning [67-69].

FRP systems use FRP composite materials, in the form of strips or sheets, as supplemental externally-bonded reinforcement. FRP systems offer advantages over traditional strengthening techniques: they are lightweight, easy to install, very thin, noncorroding, and relatively economical.

The configuration that reproduces the stirrups would consist of strips or sheets totally wrapped to the concrete section. But the tee cross-section (T-beam) or the floor (slab) prevents a closed reinforcement to be placed, because it would require breaking the flange or the floor (slab), which is particularly invasive and expensive. Actually, wrapping the entire cross-section with the FRP jacket is much less convenient than inserting new bars into the concrete, totally embedded from the top face to the bottom face of the beam, with the inclination that is wanted (vertical or at 45°).

Thus, the typical shear strengthening configuration is the U-shaped reinforcement with the ends at the bottom of the floor (slab) or of the flange. Accordingly, shear strengthening of RC beams with FRP reinforcement is typically obtained by bonding either a continuous sheet with vertical fibers or spaced vertical strips onto the web (lateral sides) of the beam.

However, U-shaped reinforcement cannot act as the tension member of the pin-joined truss, since the external reinforcement does not reach the compression zone (the top chord) or is not sufficiently anchored to the compression zone. Namely, U-shaped reinforcement does not give rise to the vertical tension ties.

The topic needs in-depth analysis to frame the problem of beam's shear strengthening (this paragraph) and midspan's shear strengthening (next paragraph) for beams without web reinforcement.

The variation of bending moment along a RC beam implies two internal forces, namely: (1) the transverse shear force across a cracked cross-section (across the concrete compression zone and crack), which is denoted by V, (2) and the bond force variation between two consecutive cracks (increase in tension force along the longitudinal reinforcement), which is denoted by ΔT_S.

In the case of RC beams without web reinforcement (no stirrups), those forces are resisted by (1) the uncracked concrete of the cracked cross-section, i.e., the concrete compression zone, (2) and the strength of the cantilever, i.e., of its built-in transverse section. According to paragraph 2, the first of those two resisting systems is kind of boosted by dowel action and aggregate interlock, while the second one is substantially boosted by dowel action and aggregate interlock.

(1) The shear strength of the uncracked concrete is dictated by concrete tensile strength. When the maximum principal stress reaches concrete tensile strength, the section reaches the maximum (ultimate) V that it can bear. A greater V causes the cracked cross-section to fail and the RC beam to collapse by oblique severing of the cracked cross-section.

(2) A cantilever fails by the bending mode, since the shear failure mode is almost always stronger although a cantilever is not slender. Failure occurs at the built-in transverse section of the concrete cantilever. The flexural strength of the cantilever is dictated by concrete tensile strength. When the maximum flexural stress (the maximum stress acting on planes transverse to the cantilever axis) reaches concrete tensile strength, the built-in horizontal section reaches the ultimate ΔT_S that it can bear. Namely, a greater ΔT_S causes the cantilever to fail and the beam to collapse by horizontal sliding of the lower part with respect to the compression upper part.

The maximum V and ΔT_S that the RC beam can bear are hence the ultimate values of the internal shear actions. The lowest of those two ultimate values is the shear strength of the RC beam and dictates the ultimate shear load.

Generally speaking, hence, increasing the shear capacity of a RC beam requires increasing the maximum V that uncracked concrete can bear, and/or the maximum ΔT_S that cantilevers can bear.

An increase in the maximum V that a cracked cross-section can bear is obtainable only by wrapping the external reinforcement around the entire cross-section, which is an inconvenient technique, as previously observed. Actually, no U-shaped reinforcement allows the maximum tolerable V to be increased, since the uncracked concrete (compression zone) lies entirely, or almost entirely, in the flange, while the external reinforcement is bonded only on the web (the ends of the reinforcement usually are at the bottom of the flange).

Ultimately, no external reinforcement allows the maximum transverse shear force V that a cracked cross-section can bear to be increased, neither around the midspan nor at the ends.

Nevertheless, in the vast majority of the RC beams, shear strength is dictated by the bond force variation ΔT_S and not by the transverse shear V.

U-shaped reinforcement can increase the maximum bond force variation ΔT_S that a cantilever can bear, since the fibers cross the cracks forming an angle different than zero.

Ultimately, the typical shear strengthening externally bonded FRP reinforcements – sheets with vertical fibers or vertical strips bonded on the web – allow, in general, the maximum bond force variation ΔT_S that can be carried by a cantilever to be increased, and, in turn, the shear strength of the beam to be increased.

Preprints (www.preprints.org) | NOT PEER-REVIEWED | Posted: 5 January 2022 doi:10.20944/preprints202201.0041.v1

4. Shear strengthening of RC beams around the midspan

The conclusion of the previous paragraph holds true if the cracks (the cantilever) and the fibers form an angle different than zero. However, typical U-shaped reinforcements form an angle equal to zero around the midspan, since there both the fibers and the cracks are vertical. Therefore, U-shaped reinforcement does not provide any increase in shear strength around the midspan, as a steel stirrup doesn't and for the same reason (Fig. 2-a).

More specifically, cracks and cantilever are vertical around the midspan. So, the only contribution of a steel stirrup would be to act as two longitudinal bars. This behavior would allow the built-in end section of the cantilever to attain the plastic hinge condition. However, the full plastic moment is lower than the cracking moment, given that the area of a stirrup is very small compared to the area of the concrete that it is embedded into. Thus, the stirrup only increases the cracking moment. However, this contribution is marginal. The same consideration can be translated to FRP with vertical fibers.

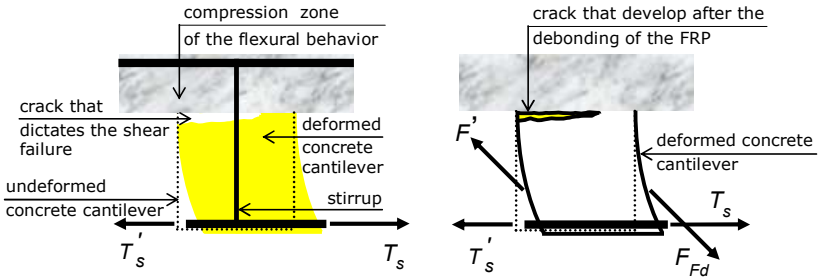

Figure 2. Concrete cantilever that dictates the capacity of the RC beam. Left: beam without side-bonded FRP reinforcement. Right: beam with side-bonded FRP reinforcement, whose fibers are at ± 45 ° (the sign of the angle depends on which of the two sides of the web the fibers are bonded to).

Ultimately, no typical U-shaped reinforcements – neither sheets with vertical fibers nor vertical strips – allow the maximum bond force variation ΔT_s tolerable by a vertical cantilever to be increased.

The pictures depicted above has proven that, in order to increase the maximum force variation ΔT_s that a vertical cantilever can bear, the reinforcement has to provide the concrete cantilever with an oblique force. Ergo, the FRP web reinforcement has to be oblique.

Analysis shows that the best fiber inclination is 45°, since that angle optimizes the behavior of the external reinforcement and makes the bond application process easy.

A series of FRP strips at 45° would not produce the intended effect, unless the spacing is unrealistically close, because a diagonal strip could pass near the tip of the crack, which would imply nil lever arm of the applied force. Thus, in order to strength in shear the beam region with vertical cracks, continuous sheets with fibers at 45° must be used. More precisely, the fibers have to be at + 45° with respect to the beam axis on the left side of the web, and at – 45° on the right side (Fig. 3). A positive angle is clockwise and vice versa.

Reinforcement should be applied onto both the lateral faces of the beam, because only onto one face would imply an asymmetric section.

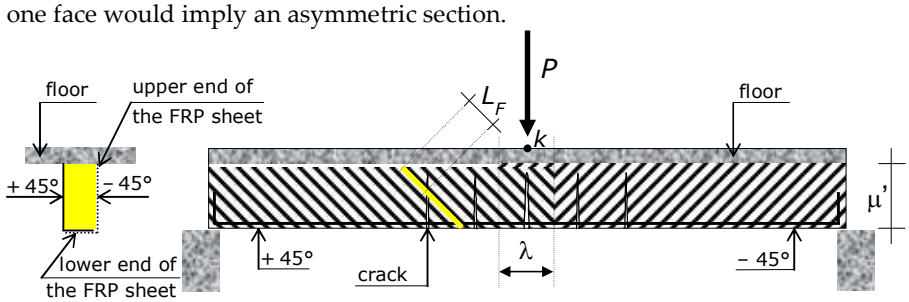

Figure 3. Externally-bonded FRP reinforcement that strengthens the RC beam subjected to a concentrated load: FRP sheets composed of unidirectional fibers at an angle of + 45° with the beam's

Preprints (www.preprints.org) | NOT PEER-REVIEWED | Posted: 5 January 2022 doi:10.20944/preprints202201.0041.v1

axis where the shear force is positive, and at – 45° where the shear force is negative. At the cross-section where the concentrated load is applied to (section *k*), the sheets overlap each other for the length $\lambda > 2 \cdot 0.707 \cdot L_{eff}$. The anchorage length (bond length) of an FRP sheet at the bottom face of the cross-section is $\lambda' > 2 \cdot 0.707 \cdot L_{eff}$. At the bottom face, a sheet overlaps the sheet attached onto the other lateral face of the concrete section (unless the web is particularly wide). The figure also shows the anchorage length L_f of a generic fiber.

If the application point of the concentrated load is not fixed but can vary its position, the sheet has to be bi-directional. Namely, a sheet with fibers at + 45° and – 45° overlapping each other, on each side of the web.

The sheet applied onto one lateral side cannot be turned up and bonded onto the other lateral side of the beam, because the fibers cannot be continuous at the lower face of the concrete section. The reason is that fiber continuity would imply an angle of + 45° at a lateral face and an erroneous angle of – 45° at the opposite lateral face (Fig. 3). In doing so, in fact, the U-shaped configuration would be effective at a lateral face but ineffective at the other lateral face.

Ultimately, two different FRP sheets must be bonded onto the two lateral faces of the RC beam.

Vertical cracks are due to the bending moment. Accordingly, the maximum width of a crack is at the bottom of the concrete section. Therefore, the fibers at the bottom are subjected to the maximum elongation, which requires them to be adequately anchored. Therefore, each FRP sheet has to be adequately anchored at the lower face of the concrete section. Unless the web is particularly wide, hence, the two side-bonded reinforcements overlap each other onto the lower face of the concrete section, and sometimes the sheet is turned up onto the opposite lateral face in order to reach the adequate bond length (Fig. 3).

The method that is herein proposed to increase the concentrated load-carrying capacity of RC beams whose load distribution has to be changed from distributed to concentrated is that described above which is also represented in Fig. 3.

The following paragraphs are devoted to presenting the analytical model that allows the concentrated load-carrying capacity of RC beams to be predicted.

5. Mechanical assumptions of the analytical model

The analytical model to predict the shear strength of the beam strengthened in the way described in the previous section relates to the reference structure that has been introduced in paragraph 2.7.

As shown by Fig. 1, which represents the reference structure, the RC beam is subjected to a concentrated load *P*, whose value may change but whose application point *g* is fixed. Point *g* is located in a part γ of the RC beam with vertical cracks. The beam is also subjected to a uniformly distributed load *q*.

According to paragraph 4, the beam is strengthened with side-bonded FRP sheets made of textile fabrics with fibers at + 45° from the left support up to point *g*, and at – 45° from the right support to point *g* (Fig. 3).

The side-bonded FRP reinforcement is composed of *N* of layers. Hereinafter, a textile fabric bonded onto a lateral face surface consists of one layer. Thus, the RC beam is strengthened by *N*/2 layers at one lateral face and *N*/2 layers at the other lateral face of the web (as previously specified, the *N*/2 layers overlap each other onto the lower face). For example, a single-layer reinforcement bonded onto both the lateral faces calls for $N = 2$.

The thickness of each layer is denoted by t_F. More specifically, t_F is the fictitious thickness of the reinforcement that, multiplied by the actual strain of the fibers and by the fictitious elastic modulus of the reinforcement, gives the force in the reinforcement per unit of width.

The model predicts the resisting shear V_{ud} (the ultimate shear force) and the maximum concentrated load P_{ud} that the RC beam can bear without triggering the shear failure mode (concentrated load-carrying capacity, apart from bending behavior).

Modeling adopts the following nomenclature (Fig. 1): L = span of the beam; M_{max} = maximum bending moment in the beam, due to q and P_{ud};(whereas the role played by q in producing M_{max} is negligible); $\beta \cdot L$ = distance of the section with M_{max} from the support that provides the beam with the maximum vertical reaction (for a point load at the midspan: $\beta = 0.5$); ξ' = crack depth; α = crack spacing; t = distance between the concrete extreme tension fiber (edge) and the center of the longitudinal bars (concrete cover), d = effective height; $\xi = \xi' - t$, which is referred to as effective crack depth.

Since the load distribution applied to the beam is changed from distributed to concentrated, P_{ud} is the main load (it is produced by dead and live loads), while q is a minor load. Around the midspan, thus, the shear force due to q is negligible with respect to the shear force due to P_{ud}. Accordingly:

$$V_{ud} = (1 - \beta) \cdot P_{ud} \quad (1)$$

Moreover, the bending moment due to q can be neglected in comparison with the bending moment due to P_{ud}. Accordingly:

$$M_{max} = \beta \cdot L \cdot V_{ud} = \beta \cdot L \cdot (1 - \beta) \cdot P_{ud} \quad (2)$$

Eq. (2) does not imply losing generality, since, in the minor cases where the distributed load q is significant, it can be modified so as to include the bending moment due to q.

Research about cracks patterns of RC beams [32, 36, 49, 55, 70, 71] supports the following two further assumptions (Fig. 1).

$$\alpha = \xi \equiv \xi' - t \quad (3) \qquad \xi = 0.67 \cdot d \quad (4)$$

The combination of assumptions (3) and (4) gives:

$$\frac{d}{\alpha} = 1.5 \quad (5)$$

The last assumption that is made is that each face of a crack is plane and remains plane also when the crack is tied by the FRP reinforcement. Accordingly, the crack profile is triangular. This is a realistic assumption as well, since the axial stiffness of the FRP reinforcement is not high, given that the thickness t_F of each layer is slight.

6. Mathematical model

This section describes the mathematical development of the model, i.e. the analytical equations.

6.1. Force in the FRP reinforcement neglecting bond-slip

The side-bonded FRP reinforcement ties (bridges) the cracks. So, opening of a crack implies stretching the FRP (Fig. 4), which produces a force in the FRP reinforcement. That force, which is denoted by F, has direction at 45°.

The strain in the FRP is induced by the crack opening. Therefore, the strain profile of the FRP at a crack is equal to the crack opening profile. By virtue of the mechanical assumptions, the FRP strain profile at a cracked section is triangular, and the strains range

Preprints (www.preprints.org) | NOT PEER-REVIEWED | Posted: 5 January 2022 doi:10.20944/preprints202201.0041.v1

from the maximum at the bottom (where the crack exhibits the maximum opening) to zero at the neutral axis (where the crack has the apex). The maximum strain, i.e., the ε at the bottom of the crack, is denoted by ε_F^{max} (Fig. 4).

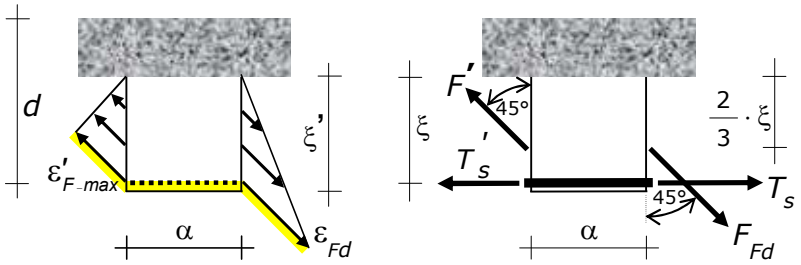

Figure 4. Concrete cantilever that fails (the midspan of the beam is on the right of the figure). On the left: strain profile in the FRP reinforcement at the two cracked sections that define the lateral sides of the concrete cantilever. The strain is linear starting from zero at the neutral axis up to ε_{Fd} at the left crack and up to $\varepsilon'_{F\text{-}max} < \varepsilon_{Fd}$ at the right crack. The FRP reinforcement bonded onto the concrete cover (which is shadowed) does not transmit any stress. On the right: forces transferred from the flexural steel reinforcement (longitudinal bars) and from the side-bonded FRP reinforcement (the fibers are at 45°) to the concrete cantilever. The latter forces consist in a resisting contribution that makes the effects of the former forces less.

The force F is produced by the triangular area of the above-described strain profile. The calculus of F makes two provisional assumptions, which will be removed in the following. The first is that there is no bond-slip between the FRP reinforcement and the concrete (not even at the bottom face, where stresses are maximum, which implies that the bottom anchorage length of the FRP reinforcement is adequate). As it is well-known, 'bond-slip' is an oxymoronic term which means the relative movement of the reinforcement with respect to the surface it is attached onto or embedded into.

The second assumption is that the FRP reinforcement coats the entire crack depth.

Under those assumptions, F turns out to be:

$$F = \frac{\varepsilon_F^{max} \cdot E_F \cdot t_F}{2} \cdot \xi' \cdot N = \frac{\varepsilon_F^{max} \cdot E_F \cdot t_F}{2} \cdot (\xi + t) \cdot N \qquad (6)$$

whose symbols have been defined in section 5.

Due to the two assumptions that have been made, F provided by (6) is the upper bound of the force. The real value of that force is lower due to some slip between the side-bonded reinforcement and the concrete lateral it is attached onto (Fig. 5). Thus, Eq. (6) will be refined in the following, so as to calculate the actual value of the force.

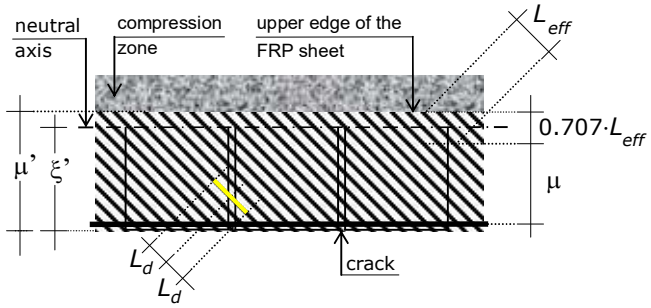

Figure 5. Fraction μ of μ′ that represents the effective height of the side-bonded FRP sheet, while the remaining part of μ′ is the anchorage length. The shadowed length $L_d + L_d$ is the length of a fiber that crack opening causes to debond.

Preprints (www.preprints.org) | NOT PEER-REVIEWED | Posted: 5 January 2022 doi:10.20944/preprints202201.0041.v1

6.2. End-debonding of the fibers

Each fiber of the FRP reinforcement spans diagonally across the lateral side of the beam's web (Fig. 3), from the upper edge (bottom of the flange) to the lower edge (bottom face of the beam).

Each fiber of the FRP reinforcement crosses a crack (infrequently two cracks). Each fiber is hence anchored at the two sides of a crack, at a certain distance from the crack. The force has to be supplied to the crack, in order to stich it. So, the bond-slip to account for is that from an end of the fiber to the crack that the fiber has to tie (to bridge). The bond-slip depends on the anchorage length of a fiber.

Since the role played by the fiber in the reinforcing system is to tie the crack, the anchorage length of a fiber is the distances between the end of the fiber and its intersection with the crack.

The two anchorages of a fiber at the two sides of the crack in general have different anchorage length. The lesser of those two anchorage lengths, which is denoted by L_F, is binding for the end-debonding. So, the model accounts for L_F.

The greater L_F the greater the strain that a fiber can reach, up to a limit called 'effective anchorage length' and denoted by L_{eff}. For $L_F \geq L_{eff}$, the stain of the fiber cannot increase anymore with respect to the ultimate limit strain, which is called 'full end-debonding strain' and is denoted by ε_{Fd}. The value of L_{eff} and ε_{Fd} can be borrowed from the literature, in particular by codes [66]:

$$L_{eff} = 0.47 \cdot \sqrt[2]{\frac{E_F \cdot t_{F\text{-}tot}}{f_{ctd}}} \quad [\text{mm}] \qquad (7)$$

$$\varepsilon_{Fd} = 0.35 \cdot \frac{\sqrt[4]{f_{cd} \cdot f_{ctd}}}{\sqrt[2]{E_F \cdot t_{F\text{-}tot}}} \qquad (8)$$

in which E_F is the elastic modulus of the FRP composites, $t_{F\text{-}tot}$ is the total thickness of the FRP reinforcement bonded onto a lateral face, f_{ctd} is the design value of the concrete cylinder tensile strength, and f_{cd} is the design value of the cylinder compressive strength of concrete.

Eqs. (7) and (8) do not incorporate E_F and $t_{F\text{-}tot}$ individually, but their product. While E_F and $t_{F\text{-}tot}$ are difficult to be defined and measured individually (actually, they are ideal quantities), their product is the axial stiffness of the FRP reinforcement, which is clearly defined and easy to be measured.

Eqs. (7) and (8) have been written in the form that is adequate for the collapse analysis, since the strength material values plugged into are those used for the ultimate limit states.

6.3. Maximum force that the FRP reinforcement can transmit to the beam

The greater L_F the greater the strain that a fiber can reach, up to a limit which is called 'effective anchorage length' and is denoted by L_{eff}. For $L_F \geq L_{eff}$, the stain of the fiber cannot increase anymore with respect to the ultimate limit strain, which is called 'full end-debonding strain' and is denoted by ε_{Fd}.

Consequently, Eq. (6) would represent the force reached by the side-bonded reinforcement at a crack if and only if (7) and (8) were satisfied, i.e., if and only if each fiber

Preprints (www.preprints.org) | NOT PEER-REVIEWED | Posted: 5 January 2022 doi:10.20944/preprints202201.0041.v1

guaranteed $L_F \geq L_{eff}$ and $\varepsilon_F^{max} \leq \varepsilon_{Fd}$. In other words, Eq. (6) is realistic only if the top and bottom edges of the side-bonded FRP reinforcement are anchored for a length L_F greater than L_{eff}. Obviously, the requirement $L_F \geq L_{eff}$ is more important at the bottom edge, where the strain is maximum, and consequently the stress is maximum as well (moreover, it has the maximum lever arm).

The requirement $L_F \geq L_{eff}$ at the bottom edge of the cross-section is obtained by bonding each FRP sheet (that on one lateral side and that on the opposite lateral side) onto the bottom face of the concrete section and, apart the case of wide web, by turning it up and bonding it onto the opposite face as well.

The requirement $L_F \geq L_{eff}$ at the top edge of the side-bonded FRP reinforcement cannot be obtained, since the flange (or the floor/slab) prevents the sheet from being prolonged beyond the crack apex for a length equal to the anchorage (and sometimes even from reaching the apex).

The anchorage length of the fiber is L_{eff}, as previously shown. However, the anchorage length of the FRP sheet is $0.707 \bullet L_{eff}$, due to the 45° angle of the fibers. The side-bonded reinforcement coats thus the entire crack only if:

$$\mu' - 0.707 \bullet L_{eff} \geq \xi' \quad (9)$$

where μ' is the length of the concrete lateral face which the sheet is bonded onto (Figs. 3, 5).

If $\mu' - 0.707 \bullet L_{eff} < \xi'$, at and near the crack apex the FRP sheet has an anchorage that does not allow the fibers to reach the full end-debonding strain. In that case, the crack is not completely tied by the side-bonded FRP reinforcement.

In that case, F is not produced by a triangular stress profile but by the area of the trapezoid inscribed into that triangle. The value of F is hence lower than that provided by Eq. (6).

The value of μ' depends on the depth of the flange (or of the floor/slab), i.e., on the depth of the web (Figs. 3, 5). The effective depth of the side-bonded FRP reinforcement is hence: $\mu = \mu' - 0.707 \bullet L_F$.

The analytical model refers to $\mu = \xi'$ and account for the actual value of μ by using a reduction factor η, which can be expressed in an analytical form. However, the analytical expression of η is really cumbersome. All the more, η has a secondary weight on the results. With all of that considered, this research work has included carrying out a parametric analysis that has provided approximate values of η. Those values are shown in Tab. 1. The values of η of Tab. 1 permit the real value of η to be replacement by an approximated value. It is to note that Tab. 1 assumes $\eta = 1$ for $\mu / \xi' > 0.80$, which is not preservative but however introduces a negligible error.

Preprints (www.preprints.org) | NOT PEER-REVIEWED | Posted: 5 January 2022 doi:10.20944/preprints202201.0041.v1

Table 1. Approximate values of η to use in lieu of the analytical exact values. The approximate values of η are expressed as a function of the μ/ξ' ratio.

$\mu/\xi' > 0.80$	$0.80 > \mu/\xi' > 0.65$	$0.65 > \mu/\xi' > 0.50$	$0.50 > \mu/\xi' > 0.35$	$0.35 > \mu/\xi' > 0.20$
$\eta = 1$	$\eta = 0.87$	$\eta = 0.77$	$\eta = 0.65$	$\eta = 0.45$

Design should guarantee $\mu/\xi' \geq 0.20$. Namely, ratios of μ/ξ' lower than 0.20 should be avoided, because would imply that only a minor part of the FRP reinforcement is well-bonded.

Eq (6) can hence be replaced by:

$$F = \frac{\varepsilon_F^{max} \cdot E_F \cdot t_F}{2} \cdot \xi' \cdot N \cdot \eta = \frac{\varepsilon_F^{max} \cdot E_F \cdot t_F}{2} \cdot (\xi + t) \cdot N \cdot \eta \quad (10)$$

Bonding the FRP reinforcement onto the cracked concrete surface poses another problem, which needs solution. A crack entails a discontinuity in the strain field of the concrete. So, around a crack the reinforcement detaches. Let L_d denote the length of the FRP reinforcement that has detached at each side of a crack (Fig. 5).

The FRP reinforcement can transfer the complete stress across a crack only by the fibers that are attached onto the concrete for a length greater than L_d. On the contrary, the fibers with anchorage length lower than L_d cannot be completely stretched. The introduction of the detachment around the crack into Eq. (10) transform that equation into (Figs. 4 and 5):

$$F = \frac{\varepsilon_F^{max} \cdot E_F \cdot t_F}{2} \cdot (\xi + t - 0.707 \cdot L_d) \cdot N \cdot \eta \quad (11)$$

Observation shows that $20 < I_d < 80$ mm [66]. On the realistic assumption that $0.70 \cdot I_d = t$, Eq. (11) turns into

$$F = \frac{\varepsilon_F^{max} \cdot E_F \cdot t_F}{2} \cdot \xi \cdot N \cdot \eta = 0.333 \cdot E_F \cdot t_F \cdot d \cdot N \cdot \eta \cdot \varepsilon_F^{max} \quad (12)$$

Let F_{Fd} denote the ultimate force in the side-bonded FRP reinforcement. Failure of the strengthened beam occurs by the end-debonding. Thus, F_{Fd} is given by the following expression:

$$F_{Fd} = \frac{\varepsilon_{Fd} \cdot E_F \cdot t_F}{2} \cdot \xi \cdot \eta \cdot N = 0.333 \cdot d \cdot \varepsilon_{Fd} \cdot E_F \cdot t_F \cdot d \cdot \eta \cdot N \quad (13)$$

According to the assumption, the side-bonded FRP reinforcement elongates in proportion to the crack width. Consequently, ε_{Fd} and F_{Fd} occurs at the crack that transmits the maximum bending moment.

The distance of the force F from the neutral axis is $2 \cdot \xi/3$ and the distance of F from the steel reinforcement is $\xi/3$.

6.4. Internal actions in the concrete cantilever

The longitudinal bond force variation ΔT_s induces the bending moment $\Delta T_s \cdot \xi$ at the built-in end of the vertical concrete cantilever (Figs. 4 and 6). The global behavior of the beam is linear-elastic (plasticity would entail displacements that would cause the FRP reinforcement to fail). So, at failure, the lever arm of the internal couple is $0.89 \cdot d$ (i.e., the distance between the center of the tension longitudinal steel and the center of the

Preprints (www.preprints.org) | NOT PEER-REVIEWED | Posted: 5 January 2022 doi:10.20944/preprints202201.0041.v1

compression stresses). Once the internal lever arm is fixed, the sole equilibrium furnishes the relation between ΔT_s and the shear action V:

$$0.89 \cdot d \cdot \Delta T_s = V \cdot \alpha \quad \rightarrow \quad \Delta T_s = \frac{V \cdot \alpha}{0.89 \cdot d} \tag{13}$$

The strain of the concrete is very small at a crack. So, it can be neglected. That being the case, the elongation of the FRP reinforcement between the crack faces (mouths) is proportional to the crack width.

The force F in the side-bonded FRP reinforcement varies along the span. At a given abscissa, F is in proportion to the width of the crack that it ties. In turn, the widths of the cracks are in proportion to the bending moment along the span. Ergo, along the span F varies in the same way as the force T_s in the longitudinal steel reinforcement (the internal lever arm is constant).

The above sequence of implications leads to the conclusion that F and T_s reach their maximum at the midspan, and that those forces decreases when the distance from the midspan increases. It follows that the variation of F at the two sides of the concrete cantilever induces a bending moment in the built-in end of the concrete cantilever that has the same sign of the bending moment induced by the variation of T_s. This fact would seem to invalidate the proposed strengthening technique.

Nevertheless, the two force T_s at the two sides of the concrete cantilever (one at a crack and at other at the consecutive crack) are coaxial. Namely, the lever arm between them is zero. On the contrary, the two forces F at the two sides of the cantilever are inclined, so the lever arm between them is different than zero. Let Ω denote the lever arm between the two forces F. (Fig. 6).

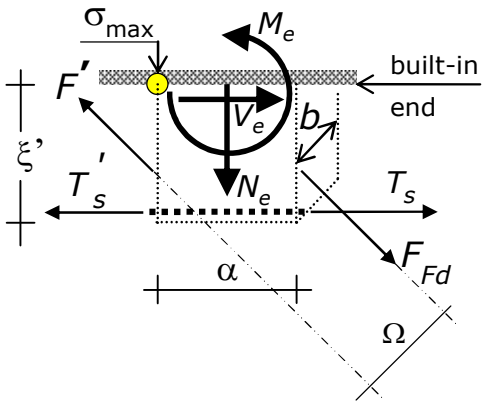

Figure 6. Forces applied to the concrete cantilever, internal actions, and maximum stress. The steel longitudinal bars and the side-bonded FRP reinforcement induce the internal actions M_e, N_e, and V_e at the built-in end of the concrete cantilever. At debonding, M_e and N_e induce the maximum tension stress σ_{max}, which is shown in the figure, including the point where that stress occurs (shadowed circle).

By virtue of Ω, the two forces F induce a bending moment whose sign is opposite to the sign of the bending moment induced by the variation of T_s, and also by the variation of the modulus of F.

As a result, the side-bonded FRP reinforcement decreases the tension stresses in the concrete cantilever due to the flexural steel reinforcement.

Ultimately, the forces that increase the strength of the concrete cantilever are F_{Fd} at the lateral side of the cantilever that is closer to the midspan and F' at the lateral side more

Preprints (www.preprints.org) | NOT PEER-REVIEWED | Posted: 5 January 2022 doi:10.20944/preprints202201.0041.v1

distant to the midspan. According to the above, $F' < F_{Fd}$ (F' will be defined in the following). Moreover, their inclination is + 45° (Figs. 2 and 4).

The forces F_{Fd} and F' induce internal actions in the concrete cantilever. At the built-in end, which is the section of the cantilever that dictates failure, the internal actions due to the FRP reinforcement are the tension axial force N_e, the transverse shear force T_e (i.e., transverse to the cantilever axis), and bending moment M_e given by the following expressions (Fig. 6).

$$N_e = \frac{\sqrt[2]{2}}{2} \cdot \left(F_{Fd} - F' \right) \qquad (14)$$

$$T_e = \frac{\sqrt[2]{2}}{2} \cdot \left(F_{Fd} - F' \right) \qquad (15)$$

$$M_e = \frac{\sqrt[2]{2}}{3} \cdot \left(F_{Fd} - F' \right) \cdot \xi - \frac{\sqrt[2]{2}}{4} \cdot \left(F_{Fd} + F' \right) \cdot \alpha \qquad (16)$$

It is to highlight that the forces of Eqs. (14) and (15) and the moment of Eq. (16) are resisting internal actions – namely, those internal actions make the internal actions in the concrete cantilever less.

Ultimately, the internal actions in the concrete cantilever are those due to the longitudinal bond force variation ΔT_s (shear force and bending moment) minus (in vectorial terms) those due to the FRP reinforcement (axial force, shear force and bending moment). Accordingly, the internal actions of Eqs. (14-16) allow the beam to carry grater concentrated loads around the midspan.

6.5. Mode of failure of the RC beam with side-bonded FRP reinforcement

Debonding of the FRP reinforcement is very brittle. When FRP reinforcement is used to strengthen in shear RC beams around the ends (at the beam's supports, where the shear demand due to distributed loads is maximum), debonding occurs before that dowel action and aggregate interlock have given substantial contributions. As a result, the actual increase in shear strength of the beam provided by the FRP reinforcement is moderate and sometimes is zero.

According to paragraph 2.5, dowel action and aggregate interlock are marginal around midspan (in fact, those effects are ignored herein). This reveals that externally-bonded FRP reinforcement is always a viable technique to strengthen in shear RC beams around the midspan (while, often, this technique does not produce the intended effects when is used to strengthen in shear RC beams around the ends).

The possible failure modes of a RC beam with side-bonded FRP reinforcement whose configuration is that described in Section 4 are *i.* cracking of the concrete cantilever *ii.* and debonding of the side-bonded FRP reinforcement. *i.* Cracking of the concrete cantilever is dictated by concrete flexural strength, which implies displaying some plastic behavior. *ii.* Debonding of the FRP reinforcement is dictated by concrete tensile strength (by mode II of fracture mechanics), which is totally brittle. Ergo, failure occurs by *ii.* debonding of the FRP reinforcement.

Failure triggers because the side-bonded FRP reinforcement stops providing the concrete cantilever with the forces F_{Fd} and F', which entails turning the resisting internal actions of Eqs. (14-16) into zero (or however into marginal values), which, in turn, causes the cantilever to fail. In fact, without the FRP reinforcement, the cantilever cannot resist the bending moment induced by the steel reinforcement at its built-in end. Once the cantilever fails, the whole beam fails.

To sum up: 1- Capacity of carrying a concentrated load applied around the midspan is dictated by debonding of the FRP reinforcement, since the cantilever, although not slender, has mainly bending behavior and it can also exhibit some plasticity. 2- FRP debonding

Preprints (www.preprints.org) | NOT PEER-REVIEWED | Posted: 5 January 2022 doi:10.20944/preprints202201.0041.v1

occurs when the maximum strain in the FRP, i.e., ε_F^{max}, reaches the debonding strain, i.e., ε_{Fd}. 3- The vertical concrete cantilever whose lateral side towards the midspan is a face of the crack where the FRP reinforcement exhibits $\varepsilon_F^{max} = \varepsilon_{Fd}$, loses the forces exchanged with the side FRP reinforcement (because the FRP reinforcement is not any longer bonded to the concrete). 4- Without the resisting forces transferred by the side FRP reinforcement to the concrete, the cantilever cannot equilibrate the bending moment produced by the variation of longitudinal force in the steel bars, i.e., the moment induced by ΔT_s at the built-in end. So, the cantilever fails, and then the beam collapses. 5- At FRP debonding, the bending moment produced by ΔT_s is resisted by two bending moments acting at the built-in section – namely, (*a*) the resisting bending moment provided by the forces in the side-bonded FRP reinforcement, (*b*) and the resisting bending moment produced by the stresses acting onto the built-in horizontal section of the cantilever.

(a) The resisting bending moment provided by the forces in the side-bonded FRP reinforcement derives from F_{Fd} and F' and their lever arm. The former force is already known, i.e., is given by Eq. (13), while the latter force is calculated in the following.

(*b*) The resisting bending moment produced by the stresses acting onto the built-in horizontal section of the cantilever requires knowing the behavior of the concrete cantilever at FRP reinforcement debonding.

Theoretical analyses carried out within this research demonstrates that at FRP debonding the maximum tension strain in the concrete cantilever is beyond the elastic limit, although always lower than the cracking tensile strain. Accordingly, the stress distribution is elasto-plastic.

Modeling assumes that stresses acting onto the built-in section at FRP debonding have a bi-triangular profile, with maximum equal to the design value of the concrete cylinder tensile strength f_{ctd}. That assumption is simultaneously realistic and conservative, because the bending moment given by the stresses that are ignored is small and increases the strength.

6.6. Maximum tension stress in the concrete cantilever induced by the loads

Let σ_{CM} denote the maximum tension stress in the concrete cantilever. The stress σ_{CM} occurs at one edge of the built-in end of the cantilever (the edge more distant from the midspan). It is induced by the bending moment (horizontal component of the internal action multiplied by the lever arm) and the axial force (vertical component of the internal action) in the concrete cantilever due to steel and FRP reinforcement (Fig. 6). On the contrary, the shear force in the cantilever (horizontal component of the internal action) does not provide any contribution to the normal stresses.

The bi-triangular profile, which implies a linear-elastic behavior of the concrete cantilever, entails that σ_{CM} is equal to:

$$\sigma_{cm} = \frac{\xi \cdot \Delta T_s}{W} + \frac{\sqrt[3]{2}}{3 \cdot W} \cdot \left(F_{Fd} - F'\right) \cdot \xi + \frac{\sqrt[3]{2}}{2 \cdot b \cdot \alpha} \cdot \left(F_{Fd} - F'\right) - \frac{\sqrt[3]{2}}{4} \cdot \left(F_{Fd} + F'\right) \cdot \frac{\alpha}{W} \quad (17)$$

where W is the section modulus of the built-in end of the concrete cantilever.

Plugging Eq. (13) into Eq. (17) leads to:

Preprints (www.preprints.org) | NOT PEER-REVIEWED | Posted: 5 January 2022 doi:10.20944/preprints202201.0041.v1

$$\sigma_{cm} = \frac{V \cdot \alpha \cdot \xi}{0.89 \cdot d \cdot W} + \frac{\sqrt[3]{2}}{3 \cdot W} \cdot \left(F_{Fd} - F'\right) \cdot \xi + \frac{\sqrt[3]{2}}{2 \cdot b \cdot \alpha} \cdot \left(F_{Fd} - F'\right) - \frac{\sqrt[3]{2}}{4} \cdot \left(F_{Fd} + F'\right) \cdot \frac{\alpha}{W} \quad (18)$$

On substituting Eq. (4) for α and ξ, Eq. (18) becomes:

$$\sigma_{cm} = \frac{0.444 \cdot V \cdot d^2}{0.89 \cdot d \cdot W} + \frac{\sqrt[3]{2} \cdot 0.667}{3 \cdot W} \cdot \left(F_{Fd} - F'\right) \cdot d + \frac{\sqrt[3]{2} \cdot 1.5}{2 \cdot b \cdot d} \cdot \left(F_{Fd} - F'\right) - \frac{\sqrt[3]{2} \cdot 0.667}{4} \cdot \left(F_{Fd} + F'\right) \cdot \frac{d}{W} \quad (19)$$

Rearranging terms, Eq. (19) can be expressed in the following form:

$$\sigma_{cm} = \frac{0.499 \cdot V \cdot d}{W} + \frac{0.314}{W} \cdot \left(F_{Fd} - F'\right) \cdot d + \frac{1.061}{b \cdot d} \cdot \left(F_{Fd} - F'\right) - 0.236 \cdot \left(F_{Fd} + F'\right) \cdot \frac{d}{W} \quad (20)$$

6.7. Gradient of the force in the side-bonded FRP reinforcement

The maximum strain in the FRP reinforcement varies at the same rate as the bending moment M. Therefore, the concrete cantilever that dictates the shear strength of the RC beam has one lateral side at the section with the maximum bending moment in the beam M_{max} due to q and P_{ud}, whereas only the latter is accounted for, while the former is neglected. If the concentrated load is at the midspan, as it is in the reference structure, the concrete cantilever that dictates the shear strength of the RC beam has one lateral side at the midspan. That lateral side is hence subjected to the moment M_{max}, which causes the side-bonded FRP reinforcement to reach the debonding strain ε_{Fd}.

The lateral side of that concrete cantilever more distant from the midspan is subjected to the moment M', which derives from the variation of M between two consecutive cracks. The moment M' causes the FRP reinforcement to reach a tension strain that is denoted by $\varepsilon'_{F\text{-}max}$.

The first modeling assumption allows the following relationship to be established: $M' = M_{max} - \alpha \cdot V_{ud}$.

Given that M_{max}, M', and ε_{Fd} are known, the strain $\varepsilon'_{F\text{-}max}$ can be derived from a proportion.

$$\varepsilon'_{F\text{-}max} = \varepsilon_{Fd} \cdot \frac{M'}{M_{max}} \quad (21)$$

Modeling assumptions allow Eq. (21) to be written in the following form:

$$\varepsilon'_{F\text{-}max} = \varepsilon_{Fd} \cdot \frac{M_{max} - \alpha \cdot V_{ud}}{M_{max}} = \varepsilon_{Fd} \cdot \left(1 - \frac{\alpha \cdot V_{ud}}{M_{max}}\right) = \varepsilon_{Fd} \cdot \left(1 - \frac{0.667 \cdot d \cdot V_{ud}}{M_{max}}\right) \quad (22)$$

Using again the modeling assumptions, Eq. (22) can be written in the following form:

Preprints (www.preprints.org) | NOT PEER-REVIEWED | Posted: 5 January 2022 doi:10.20944/preprints202201.0041.v1

$$\varepsilon'_{F\text{-}max} = \varepsilon_{Fd} \cdot \left(1 - \frac{0.667 \cdot d \cdot V_{ud}}{\beta \cdot L \cdot V_{ud}}\right) = \varepsilon_{Fd} \cdot \left(1 - \frac{0.667 \cdot d}{\beta \cdot L}\right) \quad (23)$$

The force F' in the side-bonded FRP reinforcement at the side of the concrete cantilever more distant from the midspan derives from the triangular area of the strain profile whose maximum is $\varepsilon'_{F\text{-}max}$:

$$F' = \frac{\varepsilon'_{F\text{-}max} \cdot E_F \cdot t_F}{2} \cdot \xi \cdot \eta \cdot N =$$
$$= \frac{\varepsilon_{Fd} \cdot E_F \cdot t_F}{2} \cdot 0.667 \cdot d \cdot \eta \cdot N \cdot \left(1 - \frac{0.667 \cdot d}{\beta \cdot L}\right) = \quad (24)$$
$$= \varepsilon_{Fd} \cdot E_F \cdot t_F \cdot d \cdot \eta \cdot N \cdot \left(0.333 - \frac{0.222 \cdot d}{\beta \cdot L}\right)$$

6.8. Shear strength of the RC beam in the strengthened state

According to paragraph 6.5, at failure the maximum tension stress in the concrete cantilever σ_{CM} is equal to the concrete tensile strength f_{ctd}. Plugging f_{ctd} into Eq. (20):

$$f_{ctd} = \frac{0.499 \cdot d \cdot V_{ud}}{W} + \frac{0.314}{W} \cdot \left(F_{Fd} - F'\right) \cdot d + \quad (25)$$
$$\frac{1.061}{b \cdot d} \cdot \left(F_{Fd} - F'\right) - 0.236 \cdot \left(F_{Fd} + F'\right) \cdot \frac{d}{W}$$

Eq. (25) may be solved for V_{ud}. In so doing, the ultimate shear is found:

$$V_{ud} = \frac{2 \cdot W}{d} \cdot \left[f_{ctd} - \frac{0.314}{W} \cdot \left(F_{Fd} - F'\right) \cdot d + \right. \quad (26)$$
$$\left. + 0.236 \cdot \left(F_{Fd} + F'\right) \cdot \frac{d}{W} - \frac{1.061}{b \cdot d} \cdot \left(F_{Fd} - F'\right) \right]$$

Eq. (26) may be expressed in the following form:

$$V_{ud} = \frac{2 \cdot W \cdot f_{ctd}}{d} - 0.629 \cdot \left(F_{Fd} - F'\right) + \quad (27)$$
$$+ 0.471 \cdot \left(F_{Fd} + F'\right) - \frac{2.121 \cdot W}{b \cdot d^2} \cdot \left(F_{Fd} - F'\right)$$

Modeling assumption represented by Eqs. (3-5) allow the section modulus W to be expressed as a function of the geometric parameters, which means that W is known. On substituting α into the formula of the section modulus W, it turns out to be: $W = 0.074 \cdot b \cdot d^2$. On substituting W into Eq. (27):

$$V_{ud} = \frac{0.148 \cdot b \cdot d^2 \cdot f_{ctd}}{d} - 0.629 \cdot \left(F_{Fd} - F'\right) + \quad (28)$$
$$+ 0.471 \cdot \left(F_{Fd} + F'\right) - \frac{0.157 \cdot b \cdot d^2}{b \cdot d^2} \cdot \left(F_{Fd} - F'\right)$$

Eq. (27) can be rewritten as:

$$V_{ud} = 0.148 \cdot b \cdot d \cdot f_{ctd} - 0.629 \cdot \left(F_{Fd} - F'\right) + \quad (29)$$
$$+ 0.474 \cdot \left(F_{Fd} + F'\right) - 0.157 \cdot \left(F_{Fd} - F'\right)$$

Preprints (www.preprints.org) | NOT PEER-REVIEWED | Posted: 5 January 2022 doi:10.20944/preprints202201.0041.v1

The terms given by the round brackets (one with the sign plus and two with the sign minus) can be obtained plugging Eqs. (13) and (24) into each round bracket. In so doing, the first round bracket, that with the minus sign, turns out to be:

$$F_{Fd} - F' = 0.33 \cdot d \cdot \varepsilon_{Fd} \cdot E_F \cdot t_F \cdot d \cdot \eta \cdot N - \varepsilon_{Fd} \cdot E_F \cdot t_F \cdot d \cdot \eta \cdot N \cdot \left(0.333 - \frac{0.222 \cdot d}{\beta \cdot L} \right) \quad (30)$$

Eq. (30) can be simplified into:

$$F_{Fd} - F' = 0.222 \cdot \varepsilon_{Fd} \cdot E_F \cdot t_F \cdot \eta \cdot N \cdot \frac{d^2}{\beta \cdot L} \quad (31)$$

In the same fashion, the second round bracket, that with the minus sign, can be expressed as:

$$F_{Fd} + F' = 0.333 \cdot d \cdot \varepsilon_{Fd} \cdot E_F \cdot t_F \cdot d \cdot \eta \cdot N + \varepsilon_{Fd} \cdot E_F \cdot t_F \cdot d \cdot \eta \cdot N \cdot \left(0.333 - \frac{0.222 \cdot d}{\beta \cdot L} \right) \quad (32)$$

Eq. (32) can be simplified into:

$$F_{Fd} + F' = \varepsilon_{Fd} \cdot E_F \cdot t_F \cdot \eta \cdot N \cdot \left(0.666 \cdot d - \frac{0.222 \cdot d^2}{\beta \cdot L} \right) \quad (33)$$

Plugging Eqs. (31) and (33) into (29):

$$V_{ud} = 0.148 \cdot b \cdot d \cdot f_{ctd} - 0.140 \cdot \varepsilon_{Fd} \cdot E_F \cdot t_F \cdot \eta \cdot N \cdot \frac{d^2}{\beta \cdot L} + \varepsilon_{Fd} \cdot E_F \cdot t_F \cdot \eta \cdot N \cdot \left(0.314 \cdot d - \frac{0.105 \cdot d^2}{\beta \cdot L} \right) - 0.035 \cdot \varepsilon_{Fd} \cdot E_F \cdot t_F \cdot \eta \cdot N \cdot \frac{d^2}{\beta \cdot L} \quad (34)$$

Eq. (34) allows the ultimate design resisting shear V_{ud} to be finally worked out:

$$V_{ud} = 0.148 \cdot b \cdot d \cdot f_{ctd} + 0.314 \cdot \varepsilon_{Fd} \cdot E_F \cdot t_F \cdot \eta \cdot N \cdot d - 0.280 \cdot \varepsilon_{Fd} \cdot E_F \cdot t_F \cdot \eta \cdot N \cdot \frac{d^2}{\beta \cdot L} \quad (35)$$

Eq. (35) permits the maximum concentrated load that the beam can carry to be derived. The final formula that predicts the concentrated load-carrying capacity of a RC beams P_{ud} is:

$$P_{ud} = \frac{V_{ud}}{1 - \beta} \quad (36)$$

where V_{ud} is given by Eq. (35).

Ultimately, Eqs. (35) and (36) constitute the model that allows the RC beams strengthened in the fashion described in Section 4 to be analyzed and checked against concentrated loads. In fact, the two-equations model provides the concentrated load-carrying capacity to compare to the demand.

7. Experimental verification of the model

The model is based on some assumptions, which, on one hand, are realistic, but on the other hand, suggest checking the predictive capacity of the model. Check was accomplished comparing the theoretical predictions to experimental results obtained from laboratory tests on four RC beams (Fig. 7).

Preprints (www.preprints.org) | NOT PEER-REVIEWED | Posted: 5 January 2022 doi:10.20944/preprints202201.0041.v1

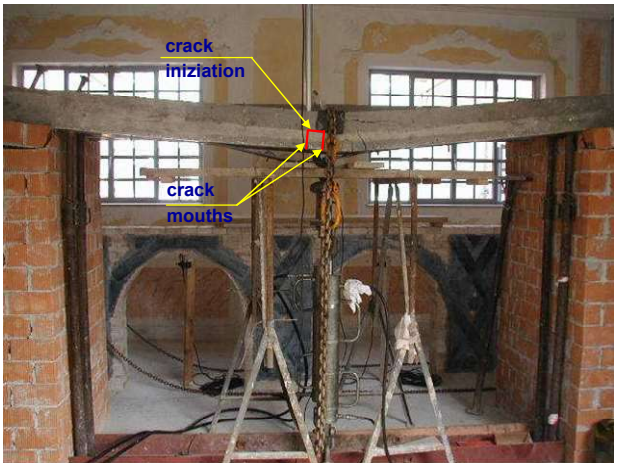

Figure 7. Experimental verification of the analytical model performed by means of four specimens. Each RC beam was subjected to a two-points load, which produced vertical cracks around the mid-span. Then, two beams were strengthened in the fashion described in Section 4, while two beams were left unreinforced. Finally, a point-load test was performed on each beam up to failure.

The beam had the same geometry, the same reinforcement and were made of the same concrete; in brief, they were identical. The height of the cross-section was 200 mm, and the width was 600 mm. Each specimen was simply-supported over a span of 3900 mm.

The beams had the minimum amount of longitudinal steel reinforcement necessary to make the cage and cast the concrete. Moreover, the beams had stirrups with a particularly large diameter. More specifically, the reinforcement consisted of 4 longitudinal steel bars with diameters of 5 mm and steel stirrups with diameter of 16 mm at the spacing of 130 mm.

The amount of longitudinal reinforcement necessary to prevent the beam from bending failure was given by longitudinal FRP strips bonded onto the entire lower face of the beam. The effective height d coincided therefore with the height of the concrete section, i.e., $d = 200$ mm.

Such a longitudinal reinforcement implied that dowel action effect was almost zero. As previously explained, the dowel action is however small where cracks are vertical. Nonetheless, that is a modeling assumption (the model disregards the dowel action). In so doing, thus, the experimental results also allowed that assumption to be verified.

Two RC beams were tested without side-bonded reinforcement, and the other two RC beams were tested with the side-bonded reinforcement described in section 4. The side-bonded reinforcement consisted of three layers of textile fabric per lateral face of the beam (i.e., $N = 6$).

The side-bonded reinforcement used for the tests consisted of cementitious matrix reinforced with continuous fibers (FRCM reinforcement). The FRCM reinforcement was preferred to the FRP reinforcement since debonding of FRCM consists of fibers that slip with respect to the matrix they are embedded into, while debonding of FRP consists of the rupture of a layer of concrete cover. That being the case, debonding of FRCM is better controllable in a laboratory test than debonding of FRP reinforcement. In particular, FRCM reinforcement allowed the debonding strain to be accurately measured, while FRP reinforcement would not have made it possible. Moreover, debonding strain of FRCM reinforcement could be accurately predicted in advance.

In detail, the value of the FRCM debonding strain ε_{Fd} that had been predicted before executing the tests was in the range 2.75 – 2.85 ‰, and the average value of the debonding strains measured in the two tests of the two FRCM reinforced beams resulted to be

2.801 ‰. Moreover, as expected, the two experimental debonding strain results were quite similar to one another.

The mechanical characteristics of the FRP reinforcement as standalone component were: t_F = 0.177 mm and E_F = 244000 N/mm^2.

The side-bonded FRP reinforcement was anchored onto the top and bottom faces of the beam, so the side-bonded FRP reinforcement guaranteed $L_F \geq L_{eff}$ both at the top and the bottom of each sheet. Accordingly, $\eta = 1$.

The concrete compressive and tensile strength measured by cylinder tests resulted to be 41.6 N/mm^2 and 4.2 N/mm^2, respectively.

Each beam was first subjected to two concentrated loads, each one applied 975 mm apart the midspan. Those symmetric forces produced vertical cracks for about 1950 mm around the midspan. Then, those two concentrated loads were taken away and the beam was strengthened in the fashion described in Section 4. Lastly, a concentrated load was applied at the midspan of each beam and was increased up to failure (Fig. 7).

The concentrated loads (forces) applied in the initial two-points load procedure and the final one-point load test used two prestressing tendons (high tensile steel cables) and two actuators – namely, one vertical prestressing tendon and actuator per side of each beam – to develop two constant vertical forces in the two-points load procedure and an increasing vertical force in the one-point load test (Fig. 7).

Ultimately, the two-points load was only the procedure to obtain RC beams with vertical cracks. So, the one-point load experiment tested four RC beams with vertical cracks around the midspan up to collapse. Two beams were tested without FRP reinforcement and two beams with side-bonded FRP reinforcement.

Failure of the two beams without the side-bonded FRCM reinforcement was triggered by the concrete cantilever at the midspam, which reached the tension crack at its built-in end.

Failure of the two beams with side-bonded FRCM reinforcement was triggered by debonding of the fibers at the midspan.

The concentrated loads that caused the two beams without FRCM side-bonded reinforcement to fail were 158.04 kN and 163.70 kN.

Setting to zero the terms of Eq. (35) that reproduce the contribution given by the side-bonded FRCM reinforcement, that equation provides V_{ud} = 74.592 kN. Since $\beta = 0.5$, Eq. (36) gives P_{ud} = 149.184 kN.

The maximum difference between the two experimental failure loads and the theoretical failure load is 8.9 %, which is marginal. Thus, the tests confirm that the stirrups are ineffective when cracks are vertical and that dowel action provides the beam with negligible strength contribution, which entails that the first term of the proposed analytical model is adequate.

It is to note that the diameter of the stirrups was large. Despite this, the stirrups do not provide the part of the beam around the midspan with any shear contribution.

The concentrated loads (forces) that caused the two beams with FRCM side-bonded reinforcement to fail were 240.40 kN and 235.18 kN.

Plugging ε_{Fd} = 2.8 ‰ into Eq. (35), that equation provides V_{ud} = 108.377 N. Since $\beta = 0.5$, Eq. (36) yields P_{ud} = 216.754 kN.

The maximum difference between the two experimental failure loads and the predicted failure load is less than 11.0 %, which is largely acceptable in order to validate the analytical model.

It can be concluded that the experimental results confirm reliability and accuracy of the analytical model (Fig. 7).

8. Two exemplificative applications of the model: theoretical predictions

Preprints (www.preprints.org) | NOT PEER-REVIEWED | Posted: 5 January 2022 doi:10.20944/preprints202201.0041.v1

The analytical model was applied to two theoretical cases. Each case study consisted of a RC beam with vertical cracks around the midspan, subjected to a concentrated load P at the midspan ($\beta = 0.5$). The geometric and mechanical characteristics of the case studies are shown in Tab. 2.

The ultimate values P_{ud} of P obtained for the two case studies allow some considerations to be made (Section 9).

Each beam is simply-supported over a span of 5500 mm and has rectangular cross section (Tab. 2). Moreover, each beam is strengthened with a side-bonded FRP reinforcement attached onto both the side surfaces for the entire span (Tab. 2). The side-bonded reinforcement is made of textile fiber at ± 45°, according to the sign of the shear. The upper edge of a sheet reaches the bottom face of the floor/slab.

Table 2. Geometric and mechanical characteristics of the two case studies. Symbols used for the rectangular sections: overall depth H, width b, effective depth d, and concrete cover t. Symbol used for the floor/slab thickness: s. Symbols used for the FRP reinforcement: elastic modulus E_F, thickness of each layer of reinforcement t_F, and total number of layers N. Symbols used for the concrete: cylinder compressive strength f_{cd} and cylinder tensile strength f_{ctd}.

H mm	b mm	d mm	t mm	s mm	t_F mm	N /	f_{cd} N/mm^2	f_{ctd} N/mm^2	E_F N/mm^2
450	150	410	40	200	0.177	3 + 3	13.2	1.14	244000
700	200	650	50	240	0.222	2 + 2	11.0	1.01	390000

8.1. First case study

On assumptions (3) and (4), the cracks exhibit the following pattern:

$$\alpha = \xi = (2/3)\cdot 410 = 273 \text{ mm} \quad (37)$$

The concrete cover is 40 mm (Tab. 2). So, crack depth is equal to $\xi' = 273 + 40 = 313$ mm. Spacing-to-depth ratio of cracks results hence to be 0.87.

The total thickness of the FRP reinforcement attached onto each side surface is $t_{F\text{-}tot} = 3\cdot 0.177 = 0.531$ mm. The effective anchorage length turns out to be:

$$L_{eff} = 0.47 \cdot \sqrt[2]{\frac{244000 \cdot 0.531}{1.14}} = 158 \text{ mm} \quad (38)$$

To obtain $L_F \geq L_{eff}$, each sheet has to be anchored onto the whole bottom side of the beam ($b = 150$ mm) and then has to be bend onto the other side of the concrete section for no less than 8 mm.

The most efficient arrangement of the side-bonded FRP reinforcement needs $\mu \geq \xi'$ i.e., $\mu' - 0.707\cdot L_{eff} \geq 313$ mm. The sheet height μ' should consequently satisfy the following relationship: $\mu' \geq 313 + 0.707\cdot 158 \Rightarrow \mu' \geq 425$ mm. Unfortunately, the floor/slab thickness bounds the height of the sheet to: $\mu' = 450 - 200 = 250$ mm < 425 mm. Given that the height of the lateral face of the concrete section is 250 mm, the condition $\mu \geq \xi'$ is therefore not obtainable.

So, each sheet is attached onto the entire height of the lateral face, to provide the side-bonded FRP reinforcement with the greatest possible value of μ'. It follows that: $\mu = 250 - 0.707\cdot 158 = 138$ mm. So, the crack depth surpasses the side-bonded FRP

reinforcement for 175 mm. This condition is accounted for by the coefficient η. The ratio μ/ξ' is therefore equal to 0.44. For μ/ξ' = 0.44, Tab. 1 gives η = 0.65.

The end-debonding strain is provided by Eq. (7):

$$\varepsilon_{Fd} = 0.35 \cdot \frac{\sqrt[4]{13.2 \cdot 1.14}}{\sqrt[2]{244000 \cdot 0.531}} = 0.00192 \quad (39)$$

The ultimate shear force is derived from Eq. (35):

$$V_{ud} = 0.148 \cdot 150 \cdot 410 \cdot 1.14 + 0.314 \cdot 0.00192 \cdot 244000 \cdot 0.177 \cdot 6 \cdot 0.65 \cdot 410 - 0.280 \cdot 0.00192 \cdot 244000 \cdot 0.177 \cdot 6 \cdot 0.65 \cdot \frac{410^2}{0.5 \cdot 5500} \quad (40)$$

from which

$$V_{ud} = 10376.3 + 41527.6 - 5521.0 = 10376.3 + 36006.6 = 46382.9 \text{ N} \quad (41)$$

The concentrated load-carrying capacity is derived from Eq. (36), plugging Eq. (42) and β = 0.5: P_{ud} = 92765.8 N ≡ 92.8 kN

The ratio between the fraction of strength due to the concrete cantilever and that due to the FRP reinforcement weighs the real role played by the side-bonded FRP reinforcement in strengthening this RC beams:

$$\frac{10376.3}{36006.6} = 0.29 = \frac{1}{3.5} \quad (42)$$

That ratio confirms that the FRP reinforcement plays the major role in providing the beam with concentrated load-carrying capacity.

Without side-bonded FRP reinforcement, P_{ud} would have been only 24.9 kN. It is to specify that P_{ud} without side-bonded FRP reinforcement was derived using a concrete flexural strength to concrete tensile strength ratio equal to 1.20.

Ultimately, the concentrated load-carrying capacity P_{ud} with side-bonded FRP reinforcement is 3.7 times greater than without external reinforcement. In other words, the side-bonded FRP reinforcement has provided an increase in P_{ud} of approximately 450 %.

This case study confirms that the proposed method is a viable strengthening technique for the cases it is devoted to.

8.2. Second case study

Assumptions (3) and (4) allow the following condition to be establish:

$$\alpha = \xi = (2/3) \cdot 650 = 433 \text{ mm} \quad (43)$$

According to Tab. 2, the concrete cover is 50 mm. The crack depth is therefore ξ' = 433 + 50 = 483 mm and the spacing-to-depth-ratio of the cracks is 0.90.

Eq. (6) gives:

$$L_{eff} = 0.47 \cdot \sqrt[2]{\frac{390000 \cdot 2 \cdot 0.222}{1.01}} = 195 \text{ mm} \quad (44)$$

 doi:10.20944/preprints202201.0041.v1

The floor/slab thickness imposes the limit $\mu' = 700 - 240 = 460$ mm to the reinforcement. On substituting the above value of μ' and L_{eff} of Eq. (44) in the relevant expression, the effective depth of the side-bonded FRP reinforcement results to be: $\mu = 460 - 0.707 \cdot 195 = 322$ mm.

The adopted side-bonded FRP reinforcement configuration implies that the crack is uncoated for 160 mm, i.e., $\mu/\xi' = 0.67$. This condition is accounted for by the coefficient η of Tab. 1. For $\mu/\xi' = 0.67$, Tab. 1 gives $\eta = 0.87$.

Eq. (7) gives:

$$\varepsilon_{Fd} = 0.35 \cdot \frac{\sqrt[4]{11.0 \cdot 1.01}}{\sqrt[2]{390000 \cdot 2 \cdot 0.222}} = 0.0015 \quad (45)$$

The ultimate shear force V_{ud} is derived from Eq. (35):

$$V_{ud} = 0.148 \cdot 200 \cdot 650 \cdot 1.01 + 0.314 \cdot 0.0015 \cdot 390000 \cdot 0.222 \cdot 4 \cdot 0.87 \cdot 650 - 0.280 \cdot 0.0015 \cdot 390000 \cdot 0.222 \cdot 4 \cdot 0.87 \cdot \frac{650^2}{0.5 \cdot 5500} \quad (46)$$

from which

$$V_{ud} = 19432.4 + 94430.6 - 19903.1 = 19432.4 + 74527.4 = 93959.8 \text{ N} \quad (47)$$

The concentrated load-carrying capacity is derived from Eq. (36), plugging Eq. (42) and $\beta = 0.5$: $P_{ud} = 187919.7$ N ≡ 187.9 kN

The ratio between the fraction of strength due to the concrete cantilever and that due to the FRP reinforcement weighs the real role played by the side-bonded FRP reinforcement in strengthening this RC beams:

$$\frac{19432.4}{74527.4} = 0.26 = \frac{1}{3.8} \quad (48)$$

That ratio confirms that the FRP reinforcement plays the major role in providing the beam with concentrated load-carrying capacity.

Without side-bonded FRP reinforcement, P_{ud} would have been only 46.6 kN. Again, P_{ud} without side-bonded FRP reinforcement was derived using a ratio between the flexural strength and the tensile strength of concrete equal to 1.20.

Ultimately, the concentrated load-carrying capacity P_{ud} with side-bonded FRP reinforcement is 4.0 times greater than without external reinforcement. In other words, the side-bonded FRP reinforcement has provided an increase in P_{ud} of approximately 400 %.

This case study confirms that the proposed method is a viable strengthening technique for the cases it is devoted to.

9. Interpretation of the results and discussions

The case studies of the preceding section, which are emblematic for beams of building, road, rail or waterway structures, show that side-bonded FRP reinforcement with fibers at ± 45° can drastically increase the concentrated load-carrying capacity of a RC beam.

The side-bonded FRP reinforcement prevents dowel action and aggregate interlock from reaching an appreciable level, and the concrete cantilever from exhibiting substantial

 doi:10.20944/preprints202201.0041.v1

plasticity. Nevertheless, the strength contributions of dowel action and aggregate interlock that are missed are irrelevant, since around the midspan concrete cracks and concrete cantilevers are vertical. Moreover, the concrete cantilever reaches however the concrete tensile strength (limit-elastic bi-triangular stress profile), whose resultant bending moment is only slightly lower than the resultant bending moment of the plastic stresses distribution at cracking of the cantilever (bi-triangular stress profile with maximum stress equal to the concrete flexural strength).

On one hand, the large increase in concentrated load-carrying capacity is due to the fact that the shear-carrying capacity around the midspan is small, and so is the concentrated load-carrying capacity, which implies a small denominator in the ratio that expresses the increase in load-carrying capacity.

On the other hand, however, the FRP reinforcement allows the concentrated load-carrying capacity to be largely increased, while it allows all the other structural capacity to be increased no more than moderately. Namely, FRP reinforcement can increase the distributed load-carrying capacity, the bending-carrying capacity, the shear-carrying capacity at the ends, the axial-carrying capacity of a column, the dissipation capacity etc., no more than moderately.

The sensitivity analysis shows that increasing the debonding strain of the side-bonded FRP reinforcement would allow the concentrated load-carrying capacity to increase in proportion. This relationship between debonding strain and capacity is however typical for any FRP reinforcement.

On one hand, the debonding strain can be increased by anchoring the FRP reinforcement with stud shear connectors [69] or by making the resin penetrate the concrete for a greater depth. The former technique can be performed by piercing the concrete under the guidance of a magnetometer survey (pacometer) which indicates the portion of concrete without steel, which can be drilled. The latter technique can be performed by applying the FRP reinforcement with a vacuum technique [69].

However, the ratio of the capacity after the strengthening and the capacity before should be not too high for any FRP reinforcement, since high ratio can be unreliable.

The model shows that the relationship between V_{ud} and d is not far from linear. That result may drive the design of the reinforcement.

10. Conclusions: review of the implications of what presented

The conventional shear capacity models of RC beams have been used for more than a century with satisfactory results, which proves their reliability. Those models have however been used mainly for new RC beams, while their use for existing RC beams started only few decades ago, i.e., less than the service life of the buildings they were used for. Moreover, the cases that the shear capacity models were applied to consisted of beams that had to carry loads higher than the original ones.

On the contrary, shear capacity models of RC beams have not been tested on beams whose load distribution has been changed from distributed to concentrated. This paper has proven that in those cases the conventional shear capacity models of RC beams fail. Not only do models fail, but also conventional strengthening techniques fail, including the most common one – namely, externally bonded FRP reinforcement.

In order to fill those gaps, the paper has presented a strengthening technique together with the predictive analytical model. The strengthening technique consist of side-bonded FRP reinforcement with fibers at 45°. The model consists of an analytical formulation that predicts the concentrated load-carrying capacity of the RC beams in the strengthened state.

The assumptions that the model is based on relate to crack spacing and crack depth. Those assumptions are in accordance with real observation, so they are realistic. Nonetheless, the expansion of the predicted shear capacity V_{ud} in a Taylor series about the

assumed conditions (i.e., $\xi = d/1.5$ and $\alpha = \xi$) proves that the error would be moderate even if ξ and α were substantially far from the assumed values.

The last significant modeling assumption is that, at debonding failure, stresses acting onto the built-in end of the concrete cantilever have a triangular distribution both in tension and compression, and that the maximum stress of the distribution is equal to concrete tensile strength. Research activity has proven that, at debonding failure, the stress distribution is elasto-plastic, which means that the assumed stress profile is both realistic and conservative.

No further substantial assumptions were made. The proposed model provides hence reliable predictions, which has been also proven by comparing theoretical predictions to experimental results.

The case studies have proven that FRP reinforcement can increase the concentrated load-carrying capacity of a RC beam substantially, i.e., up to four or five times, which is a result that FRP reinforcement cannot guarantee when used to increase other types of capacities of RC structures.

References

[1] Ritter W.,"Die Bauweise Hennebique," Schweizerische Bauzeitung, 1899; V. 33, N. 7, pp. 59-61.

[2] Morsch E., "Concrete-Steel Construction", English Translation by E. P. Goodrich, McGraw-Hill Book Company, New York, 1909, 368 pp. (Translation from third edition of Der Eisenbetonbau, first edition 1902.)

[3] Morsch E., Der Eisenbetonhau, Verlag von Konrad Wittwer, Stuttgart, 1922, 460 pp.

[4] Mörsch E.,"Der Eisenbetonbau-Seine Theorie und Anwendung (Reinforced Concrete Construction - Theory and Application)," 1920; 5th Edition, Wittwer, Stuttgart, V. 1, Part 1.

[5] Withey M. O., "Tests of Plain and Reinforced Concrete Series of 1906," Bulletin of the University of Wisconsin, Engineering Series, 1907; V. 4, N. 1, pp. 1-66.

[6] Adebar P., Zhou Z., "Bearing Strength of Compressive Struts Confined by Plain Concrete," ACI Structural Journal, 1993; V. 90, N. 5, Sept.-Oct., pp. 534-541.

[7] Al-Nahlawi K. A., Wight J. K., "Beam Analysis using Concrete Tensile Strength in Truss Models," ACI Structural Journal, 1992; V. 89, N. 3, May-June, pp. 284-289.

[8] Burdet O. L.; Sanders D. H.; Roberts C. L.; Breen J. E.; Fenves G. L., "Models and Tests of Anchorage Zones of Post-Tensioning Tendons," IABSE Colloquium on Structural Concrete, 1991; Zurich, pp. 545–550.

[9] Collins M. P., Mitchell D., Prestressed Concrete Structures, 1991, Prentice-Hall, Englewood Cliffs, N.J.

[10] Arturo Tena-Colunga; Luis AngelUrbina-Californias; Hans I. Archundia-Aranda. Assessment of the shear strength of continuous reinforced concrete haunched beams based upon cyclic testing. Journal of Building Engineering, 2017; V. 11, May, pp. 187-204.

[11] Cook W. D., Mitchell D., "Studies of Disturbed Regions near Discontinuities in Reinforced Concrete Members," ACI Structural Journal, 1998; V. 85, No. 2, Mar.-Apr., pp. 206-216.

[12] Ammar N. Hanoon; M.S. Jaafar; Salah R. Al Zaidee; Farzad Hejazi; F.N.A. Abd Aziz. Effectiveness factor of the strut-and-tie model for reinforced concrete deep beams strengthened with CFRP sheet. Journal of Building Engineering, 2017; V. 12, July, pp. 8-16.

[13] Zheng-Nan Jing, Rong-Gui Liu, Gui-Hua Xie, Dan Liu. Shear Strengthening of Deep T-Section RC Beams with CFRP Bars. Materials 2021; 14(20), 6103.

[14] Kupfer H. B., Gerstle K., "Behaviour of Concrete under Biaxial Stresses," J. Engrg. Mech. Div., ASCE, 1973; V. 99, N. 4, pp. 853-866.

[15] Leonhardt F., "Reducing the Shear Reinforcement in Reinforced Concrete Beams and Slabs," Magazine of Concrete Research, 1965; V. 17, N. 53, pp. 187-198.

[16] Leonhardt F., Walther R., "Shear Tests on Beams With and Without Shear Reinforcement," Deutscher Ausschuss für Stahlbeton, No. 151,1962, 83 pp

[17] Fudong Ma; Mingke Deng; YongYang. Experimental study on internal precast beam-column ultra-high-performance concrete connection and shear capacity of its joint. Journal of Building Engineering, 2021; V. 44, December, 103204.

[18] Muttoni A., "Applicability of the Theory of Plasticity for Dimensioning Reinforcing Concrete," PhD thesis, 1990; ETH Zurich Birkhäuser, Basel. (in German)

[19] Luciano Ombres; Salvatore Verre. Shear strengthening of reinforced concrete beams with SRG (Steel Reinforced Grout) composites: Experimental investigation and modelling. Journal of Building Engineering, 2021; V. 42, October, 103047.

[20] Reineck K.-H., "Ultimate Shear Force of Structural Concrete Members without Transverse Reinforcement Derived from a Mechanical Model," ACI Structural Journal, 1991; V. 88, N. 5, Sept.-Oct., pp. 592-602.

[21] Rogowsky D. M., MacGregor J. G., "Design of Reinforced Concrete Deep Beams," Concrete International: Design and Construction, 1986; V. 8, N. 8, Aug., pp. 49-58.

[22] Rogowsky D. M.; MacGregor J. G.; Ong S. Y., "Tests of Reinforced Concrete Deep Beams," ACI Journal, 1986; Proceedings V. 83, No. 4, July-Aug., pp. 614-623.

[23] Saumyaranjan Sahoo; Bhupinder Singh. Punching shear capacity of recycled-aggregate concrete slab-column connections. Journal of Building Engineering, 2021; V. 41, September, 102430.

[24] Schlaich J., Schäfer K., "Zur Druck-Querzug- Festigkeit des Stahlbetons," BuStb 78, 1983; H.3, pp. 73–78.

[25] Schlaich J.; Schäfer I.; Jennewein M.,"Towards a Consistent Design of Structural Concrete," Journal of the Prestressed Concrete Institute, 1987; May-June, V. 32, N. 3, pp. 75-150.

[26] Michał Szczecina, Andrzej Winnicki. Rational Choice of Reinforcement of Reinforced Concrete Frame Corners Subjected to Opening Bending Moment. Materials 2021; 14(12), 3438.

[27] Xin Yong; Zhongmin Wang; Xiaolei Li; Bo Fan. Internal force analysis of the resistance unit of frame-truss composite wall. Journal of Building Engineering, 2021; V. 44, December, 103307.

[28] Iftikhar Azim; Jian Yang; Sanjeev Bhatta; Feiliang Wang; Qing-feng Liu; Factors influencing the progressive collapse resistance of RC frame structures. Journal of Building Engineering, 2020; V. 27, January, 100986.

[29] Agus Setiya Budi, Endah Safitri, Senot Sangadji, Stefanus Adi Kristiawan. Shear Strength of HVFA-SCC Beams without Stirrups. Buildings, 2021, 11(4), 177.

[30] F. Clementi; A. Scalbi; S. Lenci; Seismic performance of precast reinforced concrete buildings with dowel pin connections. Journal of Building Engineering, 2016; V. 7, September, pp. 224-238.

[31] Claudio Ferone, Francesco Colangelo, Giuseppina Roviello, Domenico Asprone, Costantino Menna, Alberto Balsamo, Andrea Prota, Raffaele Cioffi, Gaetano Manfredi. Application-Oriented Chemical Optimization of a Metakaolin Based Geopolymer. Materials 2013, 6(5), 1920-1939; May.

[32] Hamadi Y. D., Regan P. E., "Behaviour in Shear of Beams with Flexural Cracks," Magazine of Concrete Research, 1980; V. 32, N. 1, pp. 67-77.

[33] Patrick Huber; Tobias Huber; Johann Kollegger. Influence of loading conditions on the shear capacity of post-tensioned beams with low shear reinforcement ratios. Engineering Structures, 2018; V. 170, September; pp. 91-102.

[34] Kani G. N. J., "The Riddle of Shear Failure and its Solution," ACI Journal, 1964; Proceedings V. 61, No. 4, Sept.-Oct., pp. 441-467.

[35] Seweryn Kokot. Reinforced Concrete Beam under Support Removal - Parametric Analysis. Materials, 2021, 14(20), 5917.

[36] MacGregor J. G., Walters J.R.V., "Analysis of Inclined Cracking Shear in Slender RC Beams," ACI Journal, 1967; Proceedings V. 64, pp. 644-653.

[37] Rosanna Napolitano; Antonio Bilotta; Edoardo Cosenza. Seismic lateral deformations demand in conceptual design of reinforced concrete framed structures. Journal of Building Engineering; 2012. Available online; November; 103565

[38] Tian-Feng Yuan, Se-Hee Hong, Hyun-Oh Shin, Young-Soo Yoon. Bond Strength and Flexural Capacity of Normal Concrete Beams Strengthened with No-Slump High-Strength, High-Ductility Concrete. Materials, 2020, 13(19), 4218; September.

[39] Hui Qian, Qingyuan Zhang, Xun Zhang, Enfeng Deng, Jundong Gao. Experimental Investigation on Bending Behavior of Existing RC Beam Retrofitted with SMA-ECC Composites Materials. Materials 2022, 15(1), December.

[40] Simone Ravasini, Beatrice Belletti, Emanuele Brunesi, Roberto Nascimbene, Fulvio Parisi. Nonlinear Dynamic Response of a Precast Concrete Building to Sudden Column Removal. Appl. Sci. 2021, 11(2), 599.

[41] Reineck K.-H., "Models for the Design of Reinforced and Prestressed Concrete Members," CEB Bulletin 146, 1982; Paris, pp. 43-96.

[42] Reineck K.-H., "Ultimate Shear Force of Structural Concrete Members without Transverse Reinforcement Derived from a Mechanical Model," ACI Structural Journal, 1991; V. 88, N. 5, Sept.-Oct., pp. 592-602.

[43] Jun-Hong Zhang, Shu-Shan Li, Wei Xie, Yang-Dong Guo. Experimental Study on Shear Capacity of High Strength Reinforcement Concrete Deep Beams with Small Shear Span–Depth Ratio. Materials 2020; 13(5), 1218.

[44] Lu Zhang, Tingyu Wei, Hongyu Li, Jian Zeng, Xiaofang Deng. Effects of Corrosion on Compressive Arch Action and Catenary Action of RC Frames to Resist Progressive Collapse Based on Numerical Analysis. Materials, 2021; 14(10), 2662.

[45] Chayanon Hansapinyo, Suchart Limkatanyu, Hexin Zhang, Thanongsak Imjai. Residual Strength of Reinforced Concrete Beams under Sequential Small Impact Loads. Buildings 2021, 11(11), 518.

[46] Sang-Woo Kim, Kil-Hee Kim. Prediction of Deflection of Reinforced Concrete Beams Considering Shear Effect. Materials 2021, 14(21), 6684.

[47] V. Sathish Kumar, N. Ganesan, P. V. Indira. Shear Strength of Hybrid Fibre-Reinforced Ternary Blend Geopolymer Concrete Beams under Flexure. Materials 2021, 14(21), 6634.

[48] Hasan Jasim Mohammed; Omar Khaleefah Aayeel. Flexural behavior of reinforced concrete beams containing recycled expandable polystyrene particles. Journal of Building Engineering, 2020; V. 32, November, 101805.

[49] Hongxing Zhu, Yan Zhang, Zhuhan Li, Xiaoyu Xue. Study on Crack Development and Micro-Pore Mechanism of Expansive Soil Improved by Coal Gangue under Drying–Wetting Cycles. Materials 2021, 14(21), 6546.

[50] Drucker D.C. "On Stress-Strain Relations for Soils and Load Carrying Capacity". Proc. 1st Int. Conf. Mech. of Soil Vehicle Systems, 1961; Turin.

[51] Drucker D. C. "Coulomb friction, plasticity, and limit loads", Journal of Applied Mechanics, Vol. 21, Transaction ASME, 1965; Vol. 76, pp. 71-74.

[52] Marti P., "Basic Tools of Reinforced Concrete Beam Design," ACI Journal, 1985; Proceedings V. 82, N. 1, pp. 46-56.

[53] P. Marti, "Discussion of "Basic Tools of Reinforced Concrete Design" ACI Journal, 1985; Proceedings V. 82, N. 6, Nov.-Dec., pp. 933-935.

[54] Nielsen M.P.; Braestrup M.W.; Jensen B.C.; Bach, F., "Concrete Plasticity, Beam Shear-Shear in Joints-Punching Shear," Special Publication, Danish Society for Structural Science and Engineering, 1978; Lyngby, Denmark.

[55] Nguyen Duc Tung; Christoph Betschoga; Nguyen Viet Tue. Analysis of the crack development and shear transfer mechanisms of reinforced concrete beams with low amounts of shear reinforcement. Engineering Structures, 2020; V. 222, November; 111114.

[56] Sourav Das, Iman Mansouri, Satyabrata Choudhury, Amir H. Gandomi, Jong Wan Hu. A Prediction Model for the Calculation of Effective Stiffness Ratios of Reinforced Concrete Columns. Materials 2021, 14(7), 1792.

[57] Yua P., Lia R.Q., Bie D.P., Yao X.M., Liu X.C., Duan Y.H. A coupled creep and damage model of concrete considering rate effect. Journal of Building Engineering, 2022; 45(January): 103621.

[58] Neves R., de Brito J. Estimated service life of ordinary and high-performance reinforced recycled aggregate concrete. Journal of Building Engineering; 2022. 46(April); 103769.

[59] P. Bekhta, S. Hiziroglu, O. Potapova, J. Sedliacik. Shear Strength of Exterior Plywood Panels Pressed at Low Temperature. Materials, 2009; 2(3), 876-882; August.

[60] O. Chaallal, M. Shahawy, M. Hassan. Performance of Reinforced Concrete T-Girders Strengthened in Shear with Carbon Fiber-Reinforced Polymer Fabric. ACI Structural Journal, 2002; 99(3), 335-343.

[61] Long Tang. Maintenance and Inspection of Fiber-Reinforced Polymer (FRP) Bridges: A Review of Methods. Materials, 2021; 14(24), 7826; December

[62] Triantafillou, T.C., and Antonopoulos, C.P., 2000. *Design of Concrete Flexural Members Strengthened in Shear with FRP.* ASCE J. Composites for Construction, 4(4), 198-205.

[63] A.K. Tureyen, R.J. Frosch. Concrete Shear Strength: Another Perspective.

[64] ACI PRC-440.2-17: Guide for the Design and Construction of Externally Bonded FRP Systems for Strengthening Concrete Structures. 2017

[65] fib (ceb-fip), Task group 9.3 FRP, 2001. *Externally bonded FRP reinforcement for RC structures. – Technical report on the design and use of externally bonded fiber-reinforced-polymer reinforcement (FRP EBR) for reinforced concrete structures*. Bullettin n° 14. Losanna, 513 pp.

[66] Italian National Research Council, 2004. *Guide for the Design and Construction of Externally Bonded FRP Systems for Strengthening Existing Structures - Materials, RC and PC structures, masonry structures.* Advisory Committee on Technical Recommendations for Construction.

[67] P. Foraboschi, *Predictive multiscale model of delayed debonding for concrete members with adhesively bonded external reinforcement, Composites: Mechanics, Computations, Applications 2012, 3(4): 307-329.*

[68] *P. Foraboschi. Analytical model to predict the lifetime of concrete members externally reinforced with FRP. Theoretical and Applied Fracture Mechanics, 2015; 75(1): 137-145.*

[69] *P. Foraboschi. Effectiveness of novel methods to increase the FRP-masonry bond capacity. Composites Part B: Engineering, 2016; 107(December): 214-232.*

[70] Xu R., and Liu, C., 2012. CZM-Based Debonding Simulation of Cracked Beams Strengthened by FRP Sheets. ASCE J. Eng. Mech. 138(2), 210-220.

[71] Wu, Z., Yang, S., Hu, X., Zheng, J., Fan, X., and Shan, J. 2010. Analytical Solution for Fracture Analysis of CFRP Sheet–Strengthened Cracked Concrete Beams. ASCE, J. Eng. Mech. 136, 1202.